COMPUTER VISION AND IMAGE UNDERSTANDING
Vol. 63, No. 1, January, pp. 135–144, 1996
ARTICLE NO. 0009

Parameterized Feasible Boundaries in Gradient Vector Fields

MARCEL WORRING*,† AND ARNOLD W. M. SMEULDERS

Department of Computer Science and Logic, University of Amsterdam, Kruislaan 403, 1098 SJ Amsterdam, The Netherlands

AND

LAWRENCE H. STAIB AND JAMES S. DUNCAN‡

Department of Diagnostic Radiology and Electrical Engineering, Yale University, New Haven, Connecticut 06520

Received April 7, 1994; accepted January 17, 1995

Segmentation of (noisy) images containing a complex ensemble of objects is difficult to achieve on the basis of local image information only. It is advantageous to attack the problem of object boundary extraction by a model-based segmentation procedure. Segmentation is achieved by tuning the parameters of the geometrical model in such a way that the boundary template locates and describes the object in the image in an optimal way. The optimality of the solution is based on an objective function taking into account image information as well as the shape of the template. Objective functions in literature are mainly based on the gradient magnitude and a measure describing the smoothness of the template. In this contribution, we propose a new image objective function based on directional gradient information derived from Gaussian smoothed derivatives of the image data. The proposed method is designed to accurately locate an object boundary even in the case of a conflicting object positioned close to the object of interest. We further introduce a new smoothness objective to ensure the physical feasibility of the contour. The method is evaluated on artificial data. Results on real medical images show that the method is very effective in accurately locating object boundaries in very complex images. © 1996 Academic Press, Inc.

1. INTRODUCTION

Segmentation of (noisy) images containing a complex ensemble of objects is difficult to achieve on the basis of local image information only. If a generic model of the object is available, we can pose extraction of object boundaries as a model-based segmentation procedure. This enhances the quality of segmentation, as not only local image information is used, but also the global shape of the object as captured in the model. This can be used to guarantee closed boundaries even if for some part of the boundary the image information does not indicate an edge.

As, in general, the object shape is not fixed, we need a model which is parametrically deformable. Model-based segmentation is achieved by tuning the parameters of the geometrical model in such a way that the boundary template locates and describes the object in the image in optimal way. The optimality of the solution is based on an objective function taking into account image information as well as the shape of the template. In the special case where the object shape is fixed and known, model-based segmentation reduces to standard template matching. We consider the general case here.

Apart from yielding a closed boundary, parameterized deformable templates have the important property that features of the object boundary (like its curvature) can be computed analytically from the template parameters. This reduces the considerable loss of shape information caused by the fact that edges are confined to lie on a discrete grid [12].

Model-based segmentation procedures are often used in medical imaging as the images in general are very complex, but characterized by *a priori* bounds on the shape and position of the objects. Examples are found in numerous references. In [2], ellipses are used as a model to find the left ventricle in a cardiac scintigram using a generalized Hough transform. An elliptical model is also the basis of segmentation in [5]. The ellipse is a special case of the Fourier parameterized model as used in [10]. In the latter model, *a priori* information is included as a spatial probability expressed through the likelihood of each model parameter. The probabilities are derived from a learning set

* To whom correspondence should be addressed. E-mail: worring@fwi.uva.nl.

† M. Worring was supported by the Dutch Ministry of Economic Affairs Grant 3D-Computer Vision and 3D-Image Analysis, as well as the NIH: NLM-Ep(1 R01LM05007-01A1) Grant.

‡ L. H. Staib and J. S. Duncan were partially sponsored by the NIH-NHLBI R01HL44803 Grant.

1077-3142/96 $18.00
Copyright © 1996 by Academic Press, Inc.
All rights of reproduction in any form reserved.

of parameterizations of example boundaries. A model consisting of a collection of characteristic points, connected to each other by means of springs, is used in studying deformations of the stomach [4].

In machine vision, active snakes [1, 3, 11] are in common use as flexible models. They allow for incorporation of *a priori* knowledge about corners in the contour as well as for knowledge-guided prohibited regions in the image or for regions in the image to which the snakes should be attracted. However, as will be made precise in the next section, active snakes as proposed in the references only use an implicit model. An exception is the method for snakes in [6] in which the curve is explicitly modeled using B-splines. Another set of explicit models used in computer vision are super quadrics. These have been applied in the segmentation of range images [9].

All methods, except [2], find the segmentation result in an iterative manner starting from an initial guess on the object boundary. In the iteration, for the various models, different criteria based on the shape of the object and the image data are in use as objectives.

The contributions in this paper are twofold. First, we consider the use of gradient vector fields derived from the image data through Gaussian smoothed derivatives to accurately locate the object boundary, whereas other methods use gradient magnitude only. The practical results in this paper use the model proposed in [10]. However, the use of gradient vector fields in model-based segmentation has general applicability. Second, we discover a shortcoming of all methods which treat the x- and y-coordinates of a curve separately and propose a solution. Early results on these topics were presented in [13].

This paper is organized as follows. In Section 2, we put the above-mentioned model-based segmentation in a more abstract framework and show the relations of our method to snakes. The new image objective function based on the image gradient vector field is introduced in Section 3. In Section 4, the particular template model used in this paper is presented. The proposed solution to the problems of methods which treat the x- and y-coordinates of a curve separately is given in Section 5. Implementation of the method is discussed in Section 6. Results on artificial images are given in Section 7, whereas results on real images are found in Section 8. Section 9 concludes.

2. BOUNDARY FINDING AS A GLOBAL OPTIMIZATION PROBLEM

In this introductory section, we recapitulate the principle and terminology of boundary finding as a global optimization problem.

Let $I(x, y)$ denote an image containing the object of interest and let $\mathbf{v}(t; \mathbf{p})$ be a deformable boundary template, parameterized by vector $\mathbf{p}$. The goal of our model driven segmentation procedure is to find the parameter vector $\mathbf{p}_{\text{opt}}$ such that $\mathbf{v}(t; \mathbf{p}_{\text{opt}})$ locates the object of interest in an optimal way.

The optimality of the solution is based on a global objective function $H(\mathbf{p})$ which is the line integral over the template $\mathbf{v}(t; \mathbf{p})$ of some local objective function $h(t; \mathbf{p})$:

$$H(\mathbf{p}) = \int_t h(t, \mathbf{p}) \, \|\mathbf{v}'(t)\| \, dt. \tag{1}$$

In general, the function h is based on image information, combined with information derived from the template parameters and *a priori* known shape limits of the objects.

Given an initial guess $\mathbf{p}_0$, the template is deformed by tuning the parameters to find $\mathbf{p}_{\text{opt}}$. If *a priori* information on the parameters is present, $\mathbf{p}_0$ is the average over the learning set as described in the introduction. Otherwise, $\mathbf{p}_0$ is created interactively, or by a straightforward coarse segmentation algorithm.

The segmentation procedure boils down to a (usually nonlinear) maximization problem; find the local maximum of $H(\mathbf{p})$ in the neighborhood of the initial guess $\mathbf{p}_0$:

$$\mathbf{p}_{\text{opt}} = \arg\max_{\mathbf{p}} \{H(\mathbf{p})|_{\mathbf{p}_0}\}. \tag{2}$$

This procedure should be discriminated from the use of active snakes [1, 3, 11]. In these procedures, the curve is not explicitly parameterized but, on the basis of an objective function, conditions on the derivatives of the optimal curve are derived. The latter is achieved by means of the calculus of variations.

Let $\mathbf{v}(t)$ again denote the curve of interest, but now without explicit parameterization. Then the active snakes use an energy functional which in its general form is given by

$$H(\mathbf{v}) = \int_t h(\mathbf{v}(t), \mathbf{v}'(t), \mathbf{v}''(t)) \, dt, \tag{3}$$

where as before, h indicates a local objective function based on the image characteristics and the local properties of the curve. This equation could be augmented with derivatives of higher order if needed. From Eq. (3), the Euler–Lagrange equations are derived yielding the following differential equation:

$$H_{\mathbf{v}} - \frac{\partial}{\partial t} H_{\mathbf{v}'} + \frac{\partial^2}{\partial t^2} H_{\mathbf{v}''} = 0. \tag{4}$$

Here $H_{\mathbf{v}}$ denotes differentiation of H with respect to $\mathbf{v}$. Curve estimation now becomes solving the differential equations for x and y given by Eq. (4) with initial conditions defined by the curve $\mathbf{v}_0$.

In [1, 3], the following function h is used:

$$h(\mathbf{v}(t)) = F(\mathbf{v}(t)) + \alpha(t)\|\mathbf{v}'(t)\|^2 + \beta(t)\|\mathbf{v}''(t)\|^2. \quad (5)$$

Here $F(\mathbf{v})$ is an objective function based on the image characteristics encountered along $\mathbf{v}$ and the other terms are regulating the stretching and bending of the curve, respectively. The functions α and β can be used to incorporate *a priori* shape information.

Due to the complexity of the differential equations involved the methods in [1, 3] have to use discretized derivatives of $\mathbf{v}$. This makes shape estimation, based on higher order derivatives of $\mathbf{v}(t)$, inaccurate. A better approach is followed in [6], where the curve is approximated by analytical B-splines and the analytical parameters are used in iteratively solving Eq. (4). For all the methods presented, the local objective in Eq. (5) must be such that the differential equations given by Eq. (4) are decoupled for x and y. As will appear later, this limits their use.

In this paper, we follow the approach given by Eq. (2). We will use the Fourier parameterized model for $\mathbf{p}$ (see Section 4). The function h will be based on the gradient direction in the image at every point of the boundary template and on a measure regulating the smoothness of the template.

3. IMAGE OBJECTIVE FUNCTION

Our goal is to locate the edge of the object in the image. Thus, we concentrate on the image gradient $\nabla I(x, y)$. In the literature, at this point, only the magnitude of the gradient is taken into consideration in the optimization [3, 10]. This leads to the global objective function $M(\mathbf{p})$ (an instantiation of $H(\mathbf{p})$ in Eq. (1)):

$$M(\mathbf{p}) = \int_t \|\nabla I(\mathbf{v}(t, \mathbf{p}))\| \, \|\mathbf{v}'(t)\| \, dt. \quad (6)$$

The magnitude of the gradient is a 2D scalar field. However, as is well known, more detailed information on the local image characteristics is present in the gradient as it is a 2D vector field. To illustrate, consider the case where two dark objects are located close to one another, each with a contour of the same gradient magnitude. For the objective function $M(\mathbf{p})$, the two objects locally yield an equal contribution and are equally likely to be included in the final path parameterized by $\mathbf{p}_{\text{opt}}$. So, it is undetermined where the resulting boundary will be drawn. Using the directional information of the gradient, we are able to make a distinction between the two objects, even if they are close, as the gradients point in opposite directions.

To incorporate gradient direction in the image objective function, we place a unit vector $\hat{\mathbf{n}}$ in the direction perpendicular to the boundary template (pointing outward) and consider the dot product of this vector with the image gradient. For the case considered, the dot product yields positive contributions for the object located to the inside of the template and negative contributions for the object located to the outside. Integrating the dot product of $\hat{\mathbf{n}}$ with the image gradient along the boundary template gives the objective function $D(\mathbf{p})$, measuring the local correspondence of the direction of the normal and the direction of the gradient, weighted by the magnitude of the gradient. The geometrical interpretation of the objective function is illustrated in Fig. 1.

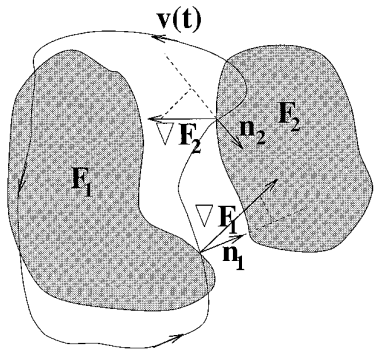

FIG. 1. Geometrical interpretation of the objective function $D(\mathbf{p})$. Two objects, F_1 and F_2 are schematically indicated by shaded areas. It is assumed that a gradient vector field ∇I is calculated where, at the boundary of each object, the gradient is a function of the corresponding object only. The vector $\hat{\mathbf{n}}$ is the unit size normal of the deformable template $\mathbf{v}(t)$. The dot product of the gradient and the normal is the size of the projection of the gradient on the line with direction equal to the normal. At position 1 the local objective is positive, whereas at position 2 the contribution is negative.

In practice, the gradient field $\nabla I(x, y)$ is estimated by Gaussian smoothed derivatives, implemented as a convolution with a Gaussian differential filter set with scale parameter σ defined as the standard deviation of the kernel. Thus, the data field ∇I and therefore the objective function are dependent on parameter σ:

$$D_\sigma(\mathbf{p}) = \pm \int_t \nabla I_\sigma(\mathbf{v}(t; \mathbf{p})) \cdot \hat{\mathbf{n}}(t; \mathbf{p}) \, \|\mathbf{v}'(t; \mathbf{p})\| \, dt. \quad (7)$$

The sign of the objective function should be positive when searching for a dark object and negative for a bright object.

Since $\hat{\mathbf{n}} = \mathbf{v}'_\perp / \|\mathbf{v}'\|$, where $\mathbf{v}'_\perp(t) = (y'(t), -x'(t))^t$, the objective function can be rewritten into

$$D_\sigma(\mathbf{p}) = \pm \int_t \nabla I_\sigma(\mathbf{v}(t; \mathbf{p})) \cdot \mathbf{v}'_\perp(t; \mathbf{p}) \, dt. \quad (8)$$

This image objective function, in principle, can also be used in the snake paradigm i.e., setting $F(\mathbf{v})$ in Eq. (5) to the integrand in Eq. (8). However, the Euler–Lagrange equations (Eq. 4) lead to a coupled system of differential

equations. Hence, the optimization method used in [3] to solve Eq. (4) is not applicable. We will therefore use the formulation as given by Eq. (2) and consequently use a different optimization method.

4. FOURIER PARAMETERIZED DEFORMABLE BOUNDARY TEMPLATES

To illustrate the use of the new image objective function we concentrate on the model as proposed in [10]. This is a very general model. It is based on the observation that for objects with closed boundaries the x- and y-coordinates of the template are periodic. Hence, a natural parameterization is by means of Fourier coefficients. The parameterization of the boundary $\mathbf{v}$ as function of the parameter t (where $t \in [0, 2\pi\rangle$) is given by

$$\mathbf{v}(t; \mathbf{p}) = \begin{pmatrix} x(t) \\ y(t) \end{pmatrix} = \begin{pmatrix} a_0 \\ c_0 \end{pmatrix} + \sum_{k=1}^{K-1} \begin{pmatrix} a_k & b_k \\ c_k & d_k \end{pmatrix} \begin{pmatrix} \cos kt \\ \sin kt \end{pmatrix}, \quad (9)$$

where the $4K - 2$ parameters describing the template are represented by the parameter vector $\mathbf{p}$:

$$\mathbf{p} = (a_0, \ldots, a_{K-1}, b_1, \ldots, b_{K-1}, c_0, \ldots, c_{K-1}, d_1, \ldots, d_{K-1})^t.$$

Given a closed curve $\mathbf{v}(t)$, its parameterization can be found using the Fourier transform:

$$\begin{bmatrix} a_0 = \frac{1}{2\pi}\int_0^{2\pi} x(t)\,dt & c_0 = \frac{1}{2\pi}\int_0^{2\pi} y(t)\,dt \\ a_k = \frac{1}{\pi}\int_0^{2\pi} x(t)\cos kt\,dt & c_k = \frac{1}{\pi}\int_0^{2\pi} y(t)\cos kt\,dt \\ b_k = \frac{1}{\pi}\int_0^{2\pi} x(t)\sin kt\,dt & d_k = \frac{1}{\pi}\int_0^{2\pi} y(t)\sin kt\,dt. \end{bmatrix} \quad (10)$$

In general, to reconstruct the curve $\mathbf{v}(t)$ exactly, one needs an infinite number of harmonics (i.e., $K = \infty$). However, in practice a limited number of harmonics suffice. As the higher harmonics are associated with high frequencies, limiting the number of harmonics yields smoother boundary templates.

The geometric interpretation of the parameters describing the template is illusrated in Fig. 2.

5. FEASIBLE TEMPLATES

The result $\mathbf{p}_{\text{opt}}$ of the optimization should represent a smooth and physically feasible template. That is, the contour should:

1. contain no cusps;
2. not be self-intersecting.

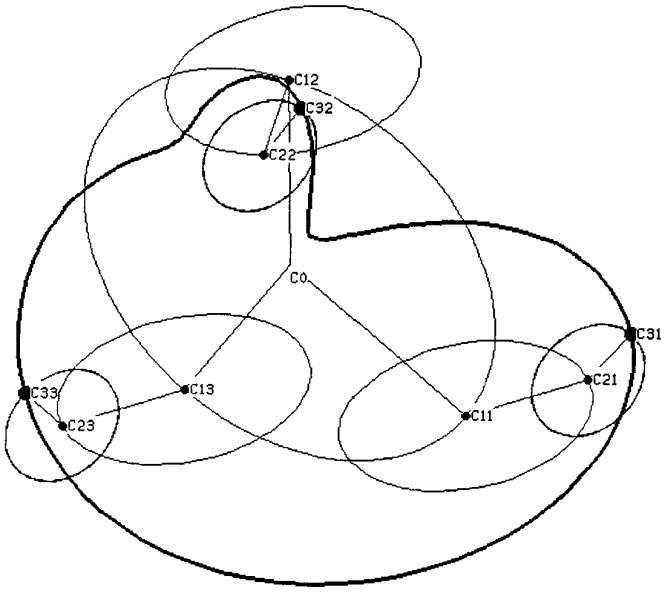

FIG. 2. The boundary $\mathbf{c}$ (dark line) is constructed using four harmonics. Harmonic 0 defines the overall position of the boundary indicated by $\mathbf{c}_0$. Harmonic 1 defines an ellipse centered at $\mathbf{c}_0$. For three different values of t, the position on the ellipse corresponding to harmonic 1 is indicated by $\mathbf{c}_{11}$, $\mathbf{c}_{12}$, and $\mathbf{c}_{13}$, respectively. The ellipse corresponding to harmonic 2 is for the three different values of t centered at $\mathbf{c}_{11}$, $\mathbf{c}_{12}$, and $\mathbf{c}_{13}$, respectively. As a function of t, the position on the boundary due to the first three harmonics is given by $\mathbf{c}_{21}$, $\mathbf{c}_{22}$, and $\mathbf{c}_{23}$. The same construction applies for the fourth harmonic leading to the final boundary.

In models that parameterize the x- and y-coordinates of the contour independently we are faced with the problem that smoothness of the coordinate functions is not a sufficient condition to prohibit cusps or self-intersections of the template. This is a consequence of ignoring the 2D shape of the template. For the Fourier parameterized templates, this is illustrated in Fig. 3. It shows that limiting the number of harmonics K of the template does control the smoothness of the coordinate functions but the template is not cusp-free. Smoothness and physical feasibility of the contour are guaranteed for the trivial case $K = 2$ (ellipses) only.

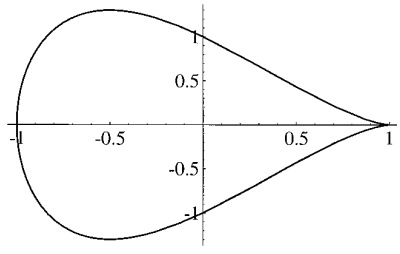

FIG. 3. The deformable template ($\cos t$, $\sin t - 1/2 \sin 2t$) composed of only three harmonics. It illustrates that whereas the two coordinate functions are each smooth, the template is not, as it shows a cusp.

As a possible solution one may intuitively wish to apply Gaussian filtering to the coordinate sequences, rather than limiting the number of harmonics. However, straightforward filtering of the coordinate sequences with a Gaussian kernel is known to yield self-intersections and cusps as well [7]. In the reference, it is argued that to avoid cusps one should repeatedly filter the sequence with Gaussian kernels with small scale parameter. In this procedure one reparameterizes the curve by arclength after each filtering step. It should be noted that taking into account arclength indeed considers the 2D nature of the curve. However, this reparameterization prohibits the use of standard optimization techniques (as will be used in this paper), as the parameters describing the curve will also be altered in this step.

Another candidate solution is to use true 2D models like star-shaped curves; however, these models tend to be much less general and hence only applicable in specific situations.

The approach followed in [10] uses probabilistic information on the parameters derived from many examples. If such information is accurate, templates having cusps or self-intersecting templates have a very low probability of occurring. Without accurate *a priori* information on the parameters, smoothness and physical feasibility have to be enforced in a different way.

We first consider cusps in the boundary and add a smoothness term to the objective function to prevent the creation of cusps. The 2D shape of the object is captured in the curvature κ of the template. Now, let $\mathbf{v}(t_0)$ be the position of a cusp. The curvature $\kappa(t_0)$ of the template is infinitely large. Further, the change of curvature $\kappa'(t_0)$ is also infinitely large. We prefer to use a smoothness contribution to the objective based on the curvature change as a mechanism to prevent cusps. In this way, regions of high curvature in the boundary are still possible. As the smoothness objective should only regulate the shape of the object, not its size, the measure has to be made independent of spatial scale. We arrive at independence by multiplication of the smoothness measure with the length of the boundary template. The resulting smoothness objective $S(\mathbf{p})$ is given by

$$S(\mathbf{p}) = \left(\int_0^{2\pi} \kappa'(\mathbf{v}(t;\mathbf{p}))^2 \,\|\mathbf{v}'(t;\mathbf{p})\|^2\, dt\right)\left(\int_0^{2\pi} \|\mathbf{v}'(t;\mathbf{p})\|^2\, dt\right). \quad (11)$$

The final objective function H_λ is a linear combination of the image objective D and the smoothness term S, with a parameter $\lambda \leq 0$ regulating the relative importance of the two:

$$H_\lambda(\mathbf{p}) = D(\mathbf{p}) + \lambda S(\mathbf{p}). \quad (12)$$

The value of λ is chosen problem-dependent.

Now, considering self-intersections of the template, we note that in the unconstrained case they appear in the process of iterative optimization in two different ways. First, given initial parameter vector $\mathbf{p}_0$, the template goes through some parameter vector $\mathbf{p}_1$, creating a cusp, before reaching the "optimal" $\mathbf{p}_{\text{opt}}$. From $\mathbf{p}_1$ and onward, the template is self-intersecting at one point. Those self-intersections cannot occur by the above prohibition. The second way occurs when the boundary intersects itself at least twice (for different values of t). Such a template can never describe a true physical boundary of an object. Either those intersections indicate that the template is attached to edges from different objects, or the boundary of the object is not followed in its natural order. Thus, these intersections provide a basis to split the template into two separate ones, or one simpler non self-intersecting template can be derived. So, after optimization, the template generated by $\mathbf{p}_{\text{opt}}$ should be examined to determine whether it is self-intersecting (where only the second way can occur) and handled based on which of the above mentioned cases occurred.

6. IMPLEMENTATION

We wish to compute the solution to the optimization problem of Eq. (2).

The image objective function $D(\mathbf{p})$ is approximated by evaluating the local objective function at N discrete points (with uniform sampling of the parameter t). Computation of the discrete points $\mathbf{v}(t_i)$ with $t_i = 2\pi i/N$ is done using the fast Fourier transform of the coordinates [8]. Derivatives of the boundary template are obtained in similar way. The points $\mathbf{v}(t_i)$ in general do not fall on gridpoints and therefore bilinear interpolation is used to estimate the gradient from the partial derivative images. The discrete formulation of the image objective becomes

$$D^*_\sigma(\mathbf{p}) = \frac{2\pi}{N}\sum_{i=0}^{N-1} \nabla I_\sigma(\mathbf{v}(t_i;\mathbf{p})) \cdot \mathbf{v}'_\perp(t_i;\mathbf{p}). \quad (13)$$

The smoothness term is approximated by

$$S^*(\mathbf{p}) = \left(\frac{2\pi}{N}\sum_{i=0}^{N-1} \kappa'(\mathbf{v}(t_i;\mathbf{p}))^2 \,\|\mathbf{v}'(t_i;\mathbf{p})\|\right)\left(\frac{2\pi}{N}\sum_{i=0}^{N-1} \|\mathbf{v}'(t_i;\mathbf{p})\|\right). \quad (14)$$

In these equations, κ' and $\mathbf{v}'$ are computed analytically from the template parameter vector $\mathbf{p}$. This should be discriminated from the estimation of derivatives in [3], where the derivatives are approximated using divided differences.

In total, the discrete formulation of (2) is given by

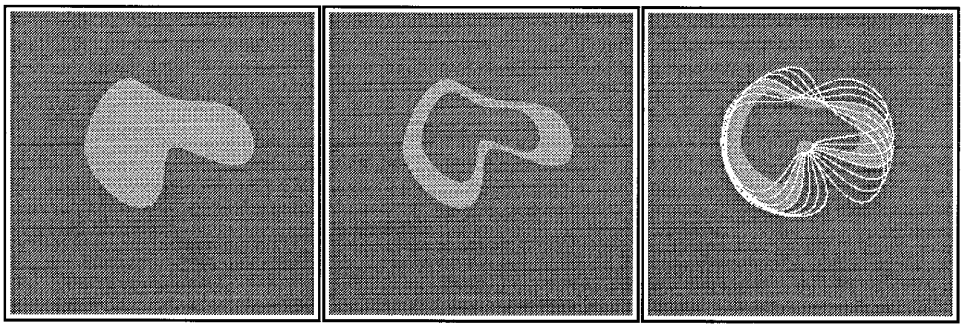

FIG. 4. The artificial images used in the experiment (256 × 256 pixels). The object in image (a) is created using a Fourier deformable template with six harmonics and has grayvalue 150 on a background of grayvalue 100. In (b), the same object is present, but now containing a large hole with the same intensity as the background. Image (c) shows the initial boundaries where from experments start.

$$\mathbf{p}^*_{\text{opt}} = \arg\max_{\mathbf{p}} \{(D^*_\sigma(\mathbf{p}) + \lambda S^*(\mathbf{p}))|_{\mathbf{p}_0}\}. \tag{15}$$

The solution to the nonlinear optimization problem is found using conjugate gradients [8]. To that end, one needs expressions for the derivative of the objective function with respect to parameter vector $\mathbf{p}$. For an element p of the parameter vector describing the x-coordinate ($p = a_0$, $p = a_k$, or $p = b_k$), the derivative of $D(\mathbf{p})$ is given by (for clarity omitting the dependence of $\mathbf{v}$ on $\mathbf{p}$ and the dependence on σ)

$$\begin{aligned}\frac{\partial D(\mathbf{p})}{\partial p} = \frac{2\pi}{N}\sum_{i=0}^{N-1} & I_{xx}(\mathbf{v}(t_i))\frac{\partial x(t_i)}{\partial p}y'(t_i) \\ & -I_{xy}(\mathbf{v}(t_i))\frac{\partial x(t_i)}{\partial p}x/(t_i) - I_y(\mathbf{v}(t_i))\frac{\partial x'(t_i)}{\partial p},\end{aligned} \tag{16}$$

with

$$\frac{\partial x(t;\mathbf{p})}{\partial a_0} = 1 \quad \frac{\partial x(t;\mathbf{p})}{\partial a_k} = \cos kt \quad \frac{\partial x(t;\mathbf{p})}{\partial b_k} = \sin kt \tag{17}$$

$$\frac{\partial x'(t;\mathbf{p})}{\partial a_0} = 0 \quad \frac{\partial x'(t;\mathbf{p})}{\partial a_k} = -\sin kt \quad \frac{\partial x'(t;\mathbf{p})}{\partial b_k} = \cos kt. \tag{18}$$

The derivative of the smoothness term is easily found from Eq. (14).

7. EXPERIMENTS

In this section, we evaluate the performance of the objective function H_λ on artificial data, in the next section we give results on real data. For comparison we also give results with the magnitude objective function as in Eq. (6) with the additional smoothness term of Eq. (11) (denoted by M_λ).

The test images used are depicted in Figs. 4a and 4b. The boundary of the object in Fig. 4a is generated from the template parameter vector $\mathbf{p}$. As starting point for the algorithm, we rotate $\mathbf{p}$ with respect to the pont (a_0, c_0) over an angle ψ, resulting in the parameter vector $\mathbf{p}_\psi$. This parameter vector is input to the optimization procedure. The initial boundaries for the values of ψ considered are shown in Fig. 4c. The goal is to retrieve the original object.

The solution $\mathbf{q}_\psi$ found by the algorithm and the parameter vector $\mathbf{p}$ are compared in terms of how close the corresponding templates are in position. To do so, one has to find a correspondence between similar points on both contours. We arrive at a correspondence by first resampling the two curves such that the curves are parameterized by arclength. Then, a fixed starting point on the first curve is taken and the corresponding starting point on the second curve is found by minimizing the overall distance between points of corresponding index. The average difference in position between corresponding points serves as our measure $E(\psi)$ of positional error between the two curves $\mathbf{p}$ and $\mathbf{q}_\psi$:

$$E(\psi) = \min_{0\le t_0<N} \frac{1}{N}\sum_{t=0}^{N-1} \|\mathbf{p}(t) - \mathbf{q}_\psi(t + t_0)\|. \tag{19}$$

We ran the algorithm and evaluated the result for the seven different starting positions as given in Figure 4. Results are shown in Fig. 5.

To verify robustness against noise, the image of Fig. 4a was subjected to additive Gaussian white noise with standard deviation γ between 0.0 and 50.0, ranging from no noise to a signal-to-noise ratio of 1. As the initial starting curve, the curve rotated over an angle of $\psi = -20°$ was selected. Results are shown in Fig. 6.

7.1. *Discussion of the Experiments*

From Fig. 5a, it is concluded that for an image containing the object without a hole, the performance of the magni-

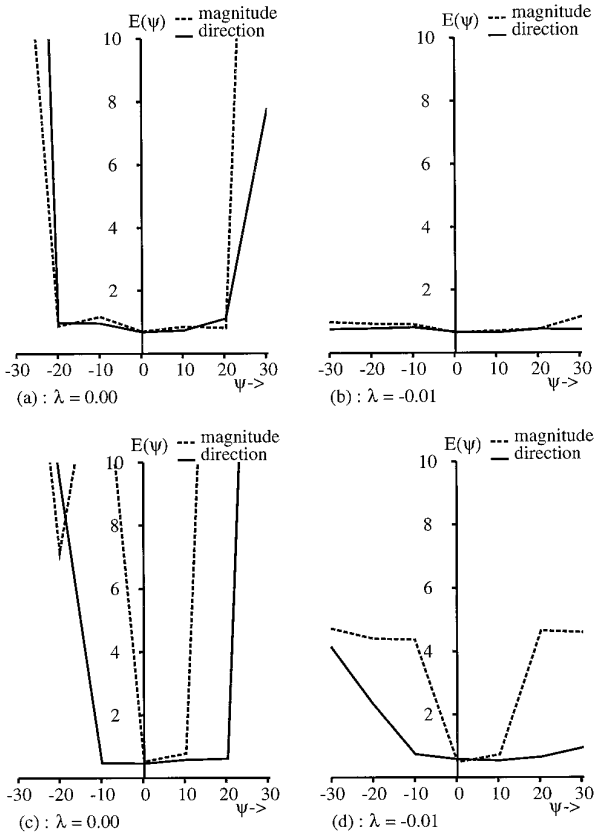

FIG. 5. The average positional error $E(\psi)$ (measured in pixels) between the original object boundary and the result of optimization: in (a) (b), for the object without a hole; in (c) (d), for the object with a hole (see Fig. 4). Input to the algorithm is the template resulting from rotation of the target boundary over an angle of ψ degrees. The gradient of the image is calculated using a Gaussian kernel with scale parameter $\sigma = 3.0$.

tude based objective M_λ and the direction based objective H_λ is approximately the same. For a large range of the rotation ψ, the object is found correctly. At the extreme values of ψ, the performance degrades dramatically. This is a direct consequence of the creation of cusps in the boundary template. Following the creation of a cusp, the template becomes self intersecting, resulting in large positional deviations. Incorporation of the smoothness term S clearly prevents the cusp creation as follows from Fig. 5b.

As a consequence of the increased complexity of the image in Fig. 4b, where only a small wall remains, performance of both objective functions degrades. However, over almost the entire range of ψ considered, the method with directed gradient now outperforms the method using gradient magnitude only. This holds for other transformations like translation and scaling as well [14].

Considering the results on noisy images (Fig. 6), it is found, as expected, that the choice of σ is a compromise between noise reduction and accurate localization of the edge. In general we can say that the global method presented is much more robust against noise than any local method.

For reasonable amounts of noise, performance is equivalent to the noise-free case if a Gaussian kernel of moderate size is used. As a consequence, it seems important to establish the effect of Gaussian smoothing on the complexity in the image due to conflicting objects and how this influences the gradient computation and subsequent optimization.

8. RESULTS ON MEDICAL IMAGES

As a first example of the practical significance of directional information we consider the segmentation of the corpus callosum from an MRI image of the brain (Fig. 7a). The selected image shows a notorious segmentation problem as the dark line separating the corpus callosum from the other image entities is very thin. Previous approaches to automated extraction found the corpus callosum by using a different objective function attracting the template to the black line rather than the edge of the object [10]. This leads to an overestimation of the actual area of

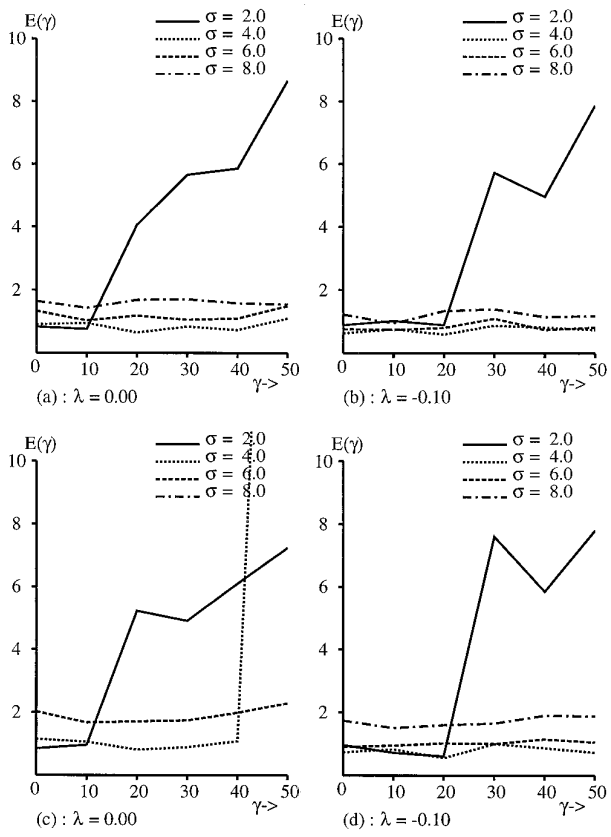

FIG. 6. For increasing noise level γ, the resulting error $E(\gamma)$ is shown for the directional objective H_λ in (a) (b) and for the magnitude-based objective M_λ in (c) (d) with ($\lambda = -0.1$). Note that in (c), one curve is not drawn, as it did not fall into the range of plotting.

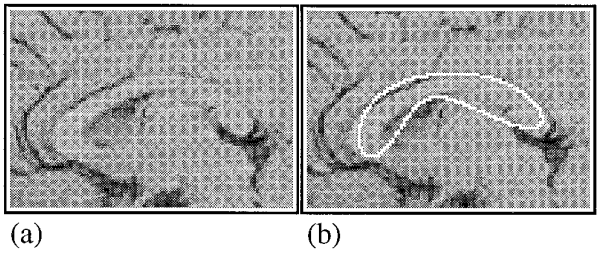

FIG. 7. An MRI image of the corpus callosum. (b) The initial boundary template represented using four harmonics.

the corpus callosum. Using directional information, we should be able to find the genuine edge.

In general when applying the model based method to an image three choices have to be made, namely the number of harmonics of the model (K), the smoothing parameter λ and the scale parameter (σ) of the Gaussian kernel used in estimating the image gradient. To illustrate the dependency on these parameters in segmentation of this particular image, we interactively defined an initial boundary and represented it using four harmonics (see Fig. 7b). We applied our method with varying number of harmonics ($K = 4, 6, 8, 16$), where at initialization the higher order harmonics not present in the initial four-harmonic template were set to zero. The smoothing parameter was also varied ($\lambda = -0.1, -0.01, -0.001, -0.0001$). The image gradient was computed with a Gaussian kernel with $\sigma = 2.0$. Results are shown in Fig. 8.

From the figure a number of interesting observations can be made. First, we see that with appropriate smoothing ($|\lambda| \geq 0.001$) the genuine edge of the corpus callosum is found except for the case $K = 16$, $\lambda = -0.1$, where only part of the boundary is found. With insufficient smoothing ($|\lambda| \leq 0.0001$) and six or more harmonics, the contour gets too much freedom in its movement and is attached to the boundaries of other objects. A second observation is, as expected, that finding smooth object boundaries can be achieved in two different ways, either by limiting the number of harmonics or by adjusting the smoothing parameter. Limiting the number of harmonics has the advantage that the method is more robust and the choice of the smoothing parameter is less critical. On the other hand, with a high number of harmonics every small detail in the contour can be followed, at the cost of reduced robustness and a more noisy curvature function. For the particular example chosen, we feel that the best compromise between conciseness to the data and smoothness is yielded by the parameter combination $K = 6$ and $\lambda = -0.001$.

As a second example, we consider finding the endocardium and epicardum of the left ventricle in an MRI image of the heart. The algorithm is started using an initial template positioned between the endocardium and epicardium (see Fig. 9a). From there, the optimization algorithm is applied, with the sign of the directional objective function used to find the epicardium (Fig. 9b) or the endocardium (Fig. 9c). The two cases are distinguished by the fact that in the first case there is a light object on a dark background, whereas in the second case there is a dark object on a light background. Note that this is the only geometric *a priori* information in use, showing the generality of the method.

The results show that the algorithm indeed is able to make the distinction between the two cases. Using the gradient magnitude only, those results can never be obtained without the use of *a priori* information. At best, the objective based on gradient magnitude finds one out of the two boundaries.

The image used is part of a temporal sequence. The algorithm was applied to six images of the sequence. Initialization is done on the first image by roughly indicating the boundary, one for the epicardium and one for the endocardium. The resulting optimized boundaries were then used as the initial boundaries for the second image, and so on. The results are shown in Fig. 10. They show that the Fourier deformable contour allows us to track the endocardium and epicardium of the left ventricle in a sequence automatically.

The time to analyze one image (or slice) is less than 30 s on a Sun sparc LX system, not yet suited for true interactive segmentation. The time is, however, dependent on the shape of the object and the initial parameters, as well as the complexity of the image. If the initial boundary is close to the final solution convergence is much faster.

9. CONCLUSION

In model-based segmentation, one optimizes an objective function based on image information and the smooth-

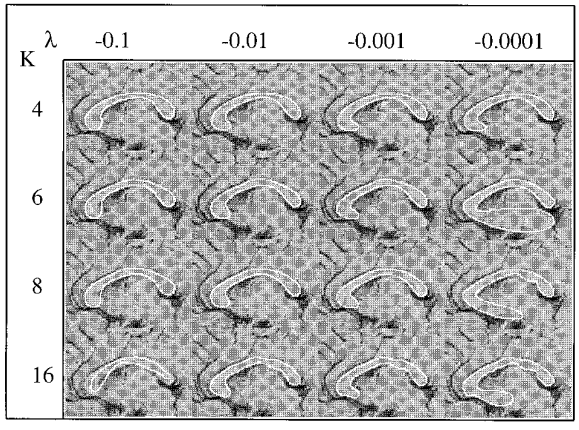

FIG. 8. Result of applying the model-based segmentation method with the initial contour as in Fig. 7(b) using varying number of harmonics K in the optimization and varying smoothing parameter λ. The scale parameter of the Gaussian kernel used in estimating the gradient was set to 2.0.

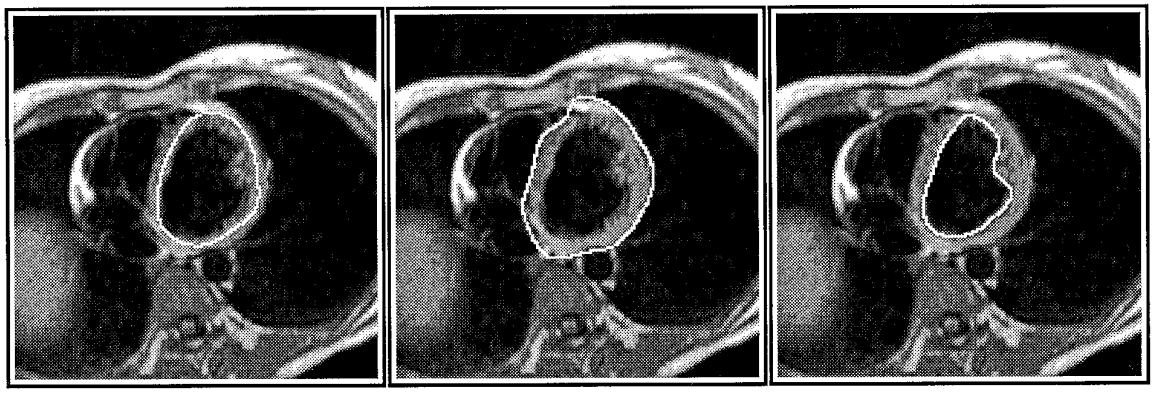

FIG. 9. The three images show the initial boundary (a) from where the algorithm is started using a six-harmonic deformable template. The second image (b) shows the result when a dark object on a light background is searched for. In the third image (c), the roles of dark and light are reversed ($\sigma = 3.0$, $\lambda = -0.01$).

ness of the template to locate an object in the image in optimal way.

Methods proposed in literature concentrate on image objectives based on the magnitude of the gradient (for example, in [3, 10]). However, as the gradient is a 2D vector field, more information is present. The method proposed in this paper, using a 2D gradient vector field derived from Gaussian smoothed derivatives of the image data as image objective, utilizes this extra information.

The power of the method is best illustrated in Fig. 9, where an initial template is placed in the middle of a small wall. By using the directional information, the method is able to make the distinction between the inside and the outside of the wall. This is not possible with any of the other methods.

Boundary templates parameterizing the *x*- and *y*-coordinates of the template separately suffer from the possible introduction of cusps in the boundary. In [10], accurate *a*

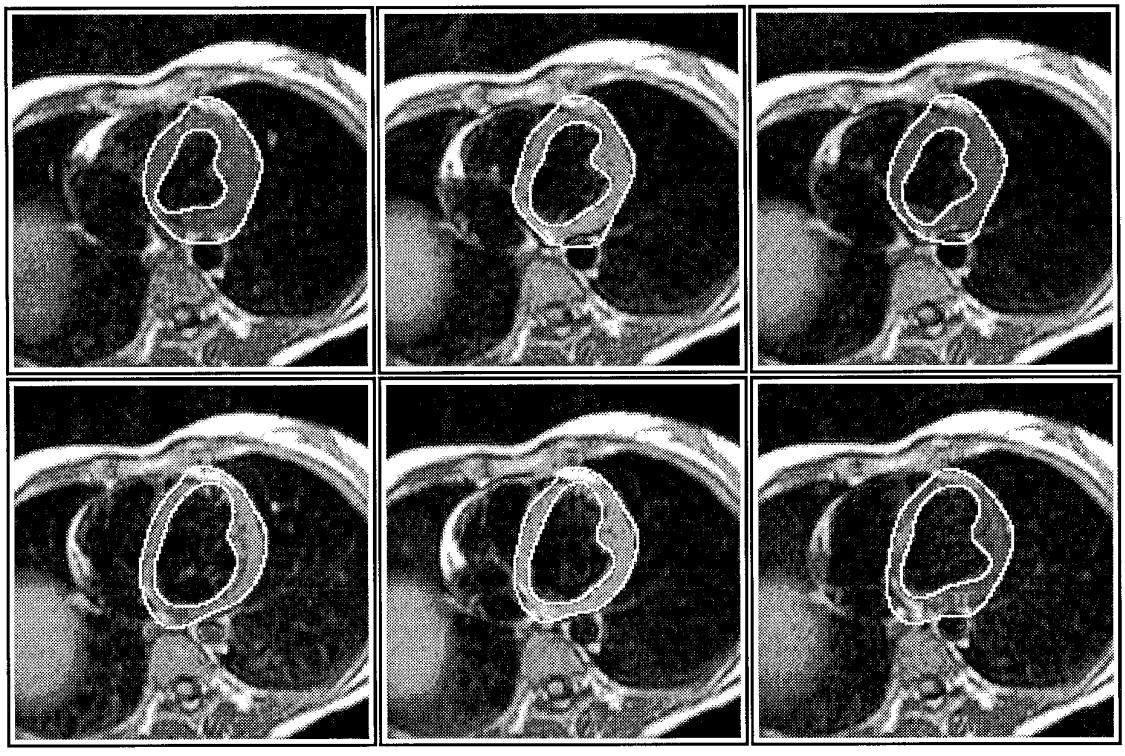

FIG. 10. The results of applying the algorithm to a sequence of images where the result of one image is used as the input for the algorithm applied to the next image in the sequence ($\sigma = 2.0$, $\lambda = -0.01$).

priori information on the parameters is assumed to prevent cusps. In this paper, we add a smoothness objective based on the 2D shape of the object. This is very effective in the prevention of cusp creation. With this additional constraint self-intersections of the template occur only if there is evidence in the image to do so and they can be detected after the boundary is found. It should be noted that prior information on the parameters is no longer essential. However, if such information is available and added as an extra objective, the quality of estimation is further improved.

Model-based segmentation enhances the quality of segmentation. With the analytically parameterized curves used, it further has the important advantage that shape calculation can be done directly from the parameters. This bypasses the inherent loss of information caused by segmentation of the image into binary regions (compare [12]).

We evaluated our method on both noise-free and noisy artificial images. The use of directional information and smoothness clearly improved the quality of segmentation. Applying the method to real data showed that the method is successful in difficult segmentation problems.

REFERENCES

1. A. A. Amini, T. E. Weymouth, and R. C. Jain, Using dynamic programming for solving variational problems in vision, *IEEE Trans. Pattern Anal. Mach. Intell.* **12**(9), 1990, 855–867.
2. J. A. K. Blokland, A. M. Vossepoel, and E. K. J. Pauwels, Delineating elliptical objects, with an application to cardiac scintigrams, *IEEE Trans. Med. Imaging*, 1987.
3. M. Kass, A. Witkin, and D. Terzopoulos, Snakes: Active contour models, *Int. J. Comput. Vision* **1,** 1988, 321–331.
4. Y. Kita, Model-driven contour extraction for physically deformed objects- application to analysis of stomach X-ray images, in *Proceedings of the ICPR, Computer Vision and Applications, The Hague, 1992,* pp. 280–284.
5. P. Lipson, A. L. Yuille, D. O'Keeffe, J. Cavanaugh, J. Taaffe, and D. Rosental, Deformable templates for feature extraction from medical images, in *First European Conference on Computer Vision, 1990,* pp. 413–417.
6. S. Menet, P. Saint-Marc, and G. Medioni, B-snakes: Implementation and application to stereo, in *Proceedings of Image Understanding Workshop, 1990,* pp. 720–726.
7. F. Mokhtarian and A. Mackworth, Scale-based description and recognition of planar curves and two-dimensional shapes, *IEEE Trans. Pattern Anal. Mach. Intell.* **8**(1), 1986, 34–43.
8. W. H. Press, B. P. Flannery, S. A. Teukolsky, and W. T. Vetterling, *Numerical Recipes,* Cambridge Univ. Press, Cambridge, UK, 1986.
9. F. Solina and R. Bajcsy, Recovery of parametric models from range images: The case for superquadrics with global deformations, *IEEE Trans. Pattern Anal. Mach. Intell.* **12**(2), 1990, 131–147.
10. L. H. Staib and J. S. Duncan, Boundary finding with parametrically deformable models, *IEEE Trans. Pattern Anal. Mach. Intell.* **14,** 1992, 1061–1075.
11. D. J. Williams and M. Shah, A fast algorithm for active contours and curvature estimation, *CVGIP: Image Understand.* **55**(1), 1992, 14–26.
12. M. Worring and A. W. M. Smeulders, Digital curvature estimation, *CVGIP: Image Understand.* **58**(3), 1993, 366–382.
13. M. Worring, A. W. M. Smeulders, L. H. Staib, and J. S. Duncan, Parameterized feasible boundaries in gradient vector fields, in *Proceedings of Information Processing in Medical Imagng* (H. H. Barrett and A. F. Gmitro, Eds.), Lecture Notes in Compuer Science, Vol. 687, pp. 48–61, Springer-Verlag, Berlin/New York, 1993.
14. M. Worring, L. H. Staib, and J. S. Duncan, *Using Smoothness and Directional Information in Fourier Parameterized Boundary Extraction*, Technical Report 92-I, Yale Univ., New Haven, CT, 1992.